Resource Allocation Policies for Battery Constrained Energy Harvesting Communication Systems with Co-Channel Interference

Iman Valiulahi, Abdelhamid Salem, *Member*, IEEE, Christos Masouros, *Senior Member*, IEEE

***Abstract*——This paper studies resource allocation policies for energy harvesting (EH) multi-user multiple input single output (MU- MISO) communication systems. The multi-antenna EH base station (BS) is equipped with a limited-capacity battery. Though employing the multi-antenna at the BS provides the channel diversity, this leads to the co-channel interference which makes the resource allocation problem hard to solve. For this challenging scenario, we first consider off-line policies based on full channel state information (CSI) and energy arrival information (EAI) to obtain the best performance for any feasible resource allocation policies. We propose an iterative algorithm using generalized linear fractional programming to obtain an optimal policy. To achieve a low-complexity sub-optimal policy, we propose another iterative algorithm using the successive convex approximation. Based on the off-line policies, we develop on-line policies in which only statistical CSI and EAI are available. The complexity of the proposed policies is derived. Finally, simulation results evaluate the performance of the proposed approaches and show that the proposed polices outperform the benchmark.**

***Index Terms*—Energy harvesting base station, on-line and off-line policies, generalized linear fractional programming, the block coordinate descent technique.**

I. Introduction

Recent cellular technologies such as 5G and 6G consume a significant amount of energy because of multiple antennas and their corresponding radio frequency (RF) chains [1], [2]. Hence, energy-efficient designs are necessary to successfully deploy these technologies. There has been a proliferation of works in the literature that studied hardware-based approaches to address this issue such as few-RF chain implementations [3], few-bit digital to analog converters (DAC)s solutions [4], and antenna selection [5]. However, these methods reduce performance metrics. Recently, EH approaches have received considerable attention in order to design systems that operate autonomously without access to the power grid as efficient methods for reducing the energy consumption costs of the future generations of communication systems [6]–[15]. In EH systems, the transmitters can harvest energy from ambient energy sources such as solar, wind, and thermoelectric sources [16]. Since these energy sources vary with time, the harvested energy will also vary over the time. For a limited storage capacity, the EH process and resource allocation techniques have to be considered carefully to optimally consume the harvested energy and improve the energy efficiency.

The authors are with the Department of Electronic and Electrical Engineering, University College London, London WC1E 7JE, U.K. (e-mails: i.valiulahi@ucl.ac.uk; a.salem@ucl.ac.uk; c.masouros@ucl.ac.uk)

Optimization problems for multiple access, broadcast, and relay channels are studied in [6], [7], and [8], respectively. In [9], to minimize the transmission time duration, the authors proposed an optimal scheduling policy for a battery with an infinite capacity. However, according to the fact that only finite energy storage capacity is available in practice, the authors in [10] extended [9] for an EH battery with a limited size capacity. The authors of [11] obtained an optimal power allocation policy in the presence of battery leakage issue. In [12], the authors provided optimal power allocation policies, for the single-user case, under the assumption of full and statistical channel state information (CSI) and energy arrival information (EAI) at the BS, which were called off-line and on-line policies, respectively. In the single user case, the authors in [13], studied power allocation policies for an EH node with processing costs. For orthogonal frequency-division multiplexing (OFDM) signaling, the authors in [14], proposed off-line and on-line power allocation policies using the binary user scheduling technique. In [17], the authors proposed the on-line and off-line policies based on a learning theoretic method. In [18], on-line power allocation techniques for device-to-device (D2D) communication systems is developed.

Traditionally, in EH multi-user communication systems, for simplicity time-division multiple access (TDMA) scheme is typically assumed. Then, using the Lagrangian theorem and Karush–Kuhn–Tucker (KKT) conditions [19], the power allocation policies were obtained. Nevertheless, TDMA operation is known to be wasteful in terms of both time and frequency resources, and is rather unrealistic in some practical scenarios [20]. In such communication systems, the users need to wait for the BS to communicate with them, leading to a substantial access delay especially when number of users is large. Multi-antenna systems can be considered as a promising solution for the multi-user communication systems since it can effectively improve data transmission [21]. Joint power scheduling and antenna selection using zero-forcing (ZF) technique for the multi-antenna EH systems in the presence of the smart grid was studied in [15] in order to provide communication services for the multi-user scenario.

However, there are still several important issues in the research on the EH multi-antenna systems, which must be addressed. First, energy and communication resource allocations are highly coupled and they are required to be jointly optimized, which is a non-convex problem and hence it is difficult to solve. Second, it is crucial to optimally consume the limited renewable energy sources to provide reliable quality of

This article has been accepted for publication in IEEE Transactions on Communications. This is the author's version which has not been fully edited and content may change prior to final publication. Citation information: DOI 10.1109/TCOMM.2022.3215997

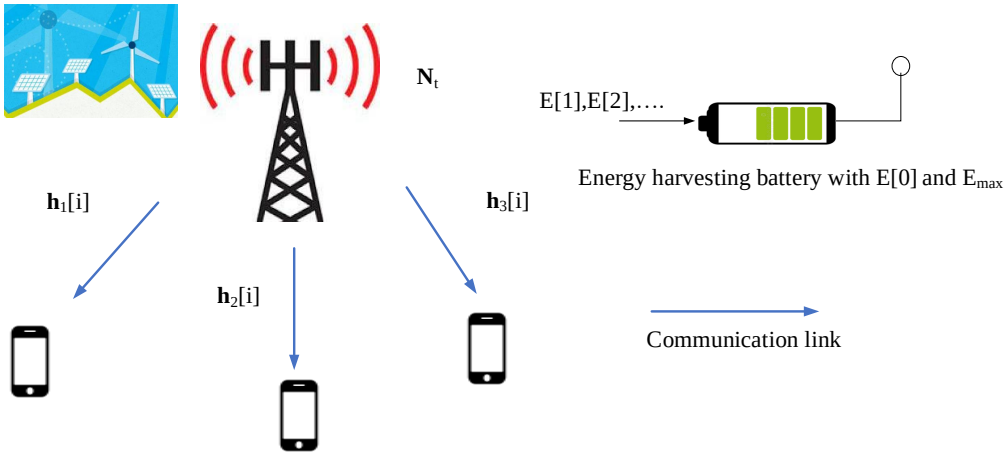

Fig. 1: A BS with N_t antennas equipped with an EH battery, communicating with M users at the i-th time slot.

service (QoS) guarantees for the users. The previous works in the literature are mainly based on the orthogonal resource allocation in both the single-antenna and multi-antenna scenarios, which can not obtain the optimal resource allocations.

Accordingly, this paper considers resource allocation policies for EH multi-user multiple input single output (MU-MISO) communication systems where the multi-antenna BS is equipped with an onboard battery with a limited energy capacity as shown in Fig. 1. In this context, we employ the energy casualty constraint which states that the harvested energy can not be consumed prior to being collected. Moreover, each user in the system has a QoS requirement in the form of a guaranteed minimum data rate. Based on this model, two scenarios are considered. First, full CSI and EAI are assumed to be available at the BS, and off-line resource allocation policies are investigated in order to obtain the best performance for any feasible resource allocation policies. In the second scenario, only statistical CSI and EAI are assumed to be known at the BS, and on-line policies are studied.

For clarity, the main contributions of this paper are summarized as follows

- We first focus on the problem of EH MU-MISO systems. Due to the presence of multiple users interference, the throughput maximization is challenging and hard to solve.
- We propose an iterative algorithm using generalized linear fractional programming (GLFP) [22] to obtain an off-line optimal policy. The convergence of the algorithm is proved. It is worth mentioning that the performance obtained by the off-line polices represents the upper bounds for any feasible resource allocation policies as full CSI and EAI is assumed to be available at the BS.
- We propose another iterative algorithm based on the successive convex approximation and block coordinate decent techniques to obtain an off-line low-complexity sub-optimal policy. We then prove that the proposed algorithm is guaranteed to converge.
- We study on-line policies in which the BS only knows statistical CSI and EAI, which can be used for practical application. Based on the derived off-line policies, the proposed on-line optimization problems are solved. The novelty of our proposed on-line policies is that they can straightforwardly apply to any CSI and EAI distributions as the first moment of CSI and EAI probability density functions (PDF)s are required.
- We investigate the computational complexity of the proposed policies.
- The numerical experiments are performed to investigate the efficiency of the proposed policies and show their superiority to the benchmark.

Similar to [23], one can estimate the CSI of each time slot by splitting the transmission time for channel estimation and serving the users. In addition, perfect EAI for solar panels is also can be obtained as the size of the solar panel and the temperature of the environment is known in advance, then the harvested energy can be estimated at the BS with a good confidence interval [24]. In this paper, however, we do not restrict our study to a single scenario and assume perfect CSI and EAI for achieving the best performance for any feasible resource allocation. Indeed, this scenario helps to compare the performance of any resource allocation technique with the optimal one. Then, by using the statistical information regarding CSI and EAI, which can be obtained by a long-term measurement, we develop on-line policies which can be exploited in practice.

We show that our proposed policies achieve better performance than the ZF precoding in terms of the average throughput. This is because of the fact that our proposed policies directly obtain the optimal beamforming vectors. We also show that the performance of the proposed on-line scenario with the imperfect CSI and EAI is comparable with the off-line scenarios, which highlights the practical aspects of the proposed policies. In addition, the low complexity sub-optimal solutions achieve almost similar performance as the optimal policies. We also demonstrate that the performance of

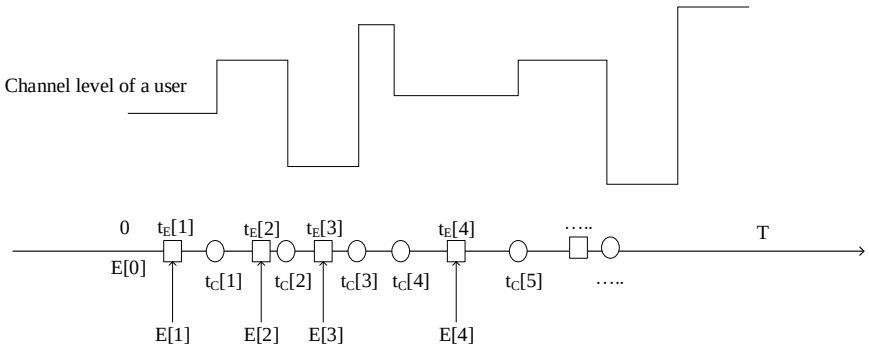

Fig. 2: An illustration of channel level changes and energy arrivals.

the resource allocation can be improved by employing an EH battery with a larger size.

The paper is organized as follows: The system model and problem formulation are presented in Section II. Section III is devoted to the off-line optimal and low-complexity sub-optimal policies. The on-line optimal and low-complexity sub-optimal policies are studied in Section IV. The overall computational costs of the proposed policies are derived in Section V. Section VI is allocated to numerical experiments. Finally, the paper is concluded in Section VII.

Throughout the paper, scalars, vectors, and matrices are denoted by lowercase, lowercase boldface, and uppercase boldface letters, respectively. The operators $(\cdot)^T$, $(\cdot)^H$, and $\mathbb{E}\{\cdot\}$ represent the transpose of a vector, the hermitian of a vector, and the expectation of a random process, respectively. The absolute value and norm two of a vector is denoted by $|\cdot|$ and $\|\cdot\|$, respectively. We use the symbol $\emptyset$ to show an empty set. The interior point of the set ω is denoted by intω.

II. System Model and Problem Formulation

We consider a down-link EH MU-MISO system with N_t antennas equipped with a limited size battery with the maximum capacity $E_{\max}$ that serves M single antenna users, as shown in Fig. 1. Let $\mathcal{M} = \{1, \cdots, M\}$ be the set of the users. In Fig. 2, we demonstrate an example of the channel changes and energy arrival rates over the transmission time. As shown in this figure, we assume that the transmission interval is $[0, T)$ and the energy arrival, T_E, follows a Poisson process with rate λ_E and energy values, $E[i]$ for $i \in \{1, \cdots, T_E\}$, are uniformly distributed in the interval $[E_{\min}[i], E_{\max}[i]]$, i.e., $E[i] \backsim U(E_{\min}[i], E_{\max}[i])$ for $i \in \{1, \cdots, T_E\}$. Hence, the times of energy arrivals are $\{t_E[1], \cdots, t_E[T_E]\}$ in values of $\{E[1], \cdots, E[T_E]\}$. The available energy in the battery at the time 0 is $E[0]$. An illustration of these parameters are shown in Fig. 2. Inline with [13], [14], [17], we use a full duplex battery which can be charged and discharged at the same time. Similarly, the number of changes in the channel states, T_C, are modeled as a Poisson process with rate λ_C, which results in the set $\{t_C[1], \cdots, t_C[T_C]\}$ for the channel changes during the transmission interval. As shown in Fig. 2, block fading channel is assumed in this paper, where the channel fading level is constant during each block ($0 < t \leq t_C[1]$) and it changes after each time interval independently ($t_C[1] < t \leq t_C[2]$). Thus, the time of channels in channel states for each event is related to the coherence time of the channel. For ease of notation, as shown in Fig. 2, we assume that all users experience the same coherence time. Our model can be generalized to different coherence times for all users at the cost of more complex parameters. Let us define a change of the channel for users or energy arrivals as an event and the time duration between two consecutive events as a time slot. Using the number of energy arrivals and channel changes, we have $K = T_C + T_E$ events happen over the transmission interval. Regarding the fact that merging two independent Poisson processes with rates λ_1 and λ_2, respectively, is still a Poisson process with the rate $\lambda_1 + \lambda_2$, number of events is a Poisson process with rate $\lambda_E + \lambda_C$. Consequently, the time slots can be written as $\ell[i] = t[i] - t[i-1]$, $\forall i \in \mathcal{K} = \{1, 2, \cdots, K+1\}$ which constructs the vector $\boldsymbol{\ell} \in \mathbb{R}^{(K+1)\times 1}$. Note that the last time slot is associated with the last event and the end of the transmission interval. For ease of notation, we define $\boldsymbol{t}_E = [t_E[1], \cdots, t_E[T_E]]^T$, $\boldsymbol{E} = [E[1], \cdots, E[T_E]]^T$, and $\boldsymbol{t}_C = [t_C[1], \cdots, t_C[T_C]]^T$. As shown in Fig. 1, $\boldsymbol{h}_m[i] \in \mathbb{C}^{N_t \times 1}$ is the complex channel state vector for the m-th user at the i-th time slot. We adapt the resource allocation policy $K+1$ times at the BS over $[0, T)$. Note that Poisson process with uniform value can cover other practical energy arrival models such as Bernoulli and i.i.d studied in [18].

Using a linear transmission scheme, where the BS sends M independent data streams at each time slot, the achievable throughput for the m-th user at the i-th time slot can be expressed as

$$R_m[i] = B \log_2 \big(1 + \gamma_m[i]\big), \tag{1}$$

where B is the bandwidth and $\gamma_m[i]$ is the signal-to-interference-plus-noise ratio (SINR) which can be written as

$$\gamma_m[i] = \frac{|\boldsymbol{h}_m^H[i]\boldsymbol{w}_m[i]|^2}{\sum_{j\neq m}^{M} |\boldsymbol{h}_m^H[i]\boldsymbol{w}_j[i]|^2 + \sigma^2}, \tag{2}$$

where $\sigma^2 = N_0 B$ is the power of additive white Gaussian noise (AWGN) in which N_0 is its spectral density and $\boldsymbol{w}_m[i] \in \mathbb{C}^{N_t \times 1}$ is the precoding vector for the m-th user at

the $i-$th time slot. The term $\sum_{j\neq m}^{M}|\boldsymbol{h}_m^H[i]\boldsymbol{w}_j[i]|^2$ represents the co-channel interference of other users at the m-th user and the i-th time slot. Since the harvested energy can not be consumed prior to being harvested, any feasible transmission policy should satisfy the following constraints [10]

$$\sum_{i=1}^{k}\left(\sum_{m=1}^{M}\|\boldsymbol{w}_m[i]\|^2\right)\ell[i]\leq\sum_{i=1}^{k}E_{in}[i],\quad k\in\mathcal{K},\tag{3}$$

where $E_{in}[1]=E[0]$, $E_{in}[i]=E[\cdot]$ if the i-th event is an energy arrival and $E_{in}=0$ if the event is a change of the channel level, constructing the vector $\boldsymbol{E}_{in}=[E_{in}[1],\cdots,E_{in}[K+1]]^T$ (see Fig. 2). These constraints are known as energy casualty. On the other hand, all the harvested energy should be utilized for communication purposes to avoid battery overflows which can be expressed by the following constraints [10]

$$\sum_{i=1}^{k}\left(\sum_{m=1}^{M}\|\boldsymbol{w}_m[i]\|^2\right)\ell[i]\geq\sum_{i=1}^{k}E_{in}[i]-E_{\max},\quad k\in\mathcal{K}.\tag{4}$$

Our target is to maximize the average throughput over the transmission time subject to the energy and user scheduling constraints while guaranteeing a minimum rate as a QoS requirement of the users. Accordingly, the optimization problem for this case can be formulated as

$$\begin{aligned}\max_{\substack{\boldsymbol{w}_1[i],\cdot,\boldsymbol{w}_M[i]\\ \text{for } i=\{1,\cdots,K+1\}}}\quad&\frac{1}{(K+1)M}\sum_{i=1}^{K+1}\sum_{m=1}^{M}R_m[i]\\ &\text{s.t. }(3),\ (4),\\ &R_m[i]\geq R^{\mathrm{q}},\quad\forall\ m,i,\end{aligned}\tag{5a}$$

where R^q is the minimum data requested by the users. Constraint (5a) is for the QoS requirements. Solving problem (5) is challenging because of the non-convex objective value and the entanglement of the beamforming vectors in both numerator and denominator of the SINR fraction in (5a). However, in Section III, we provide optimal and low-complexity sub-optimal policies for this problem, respectively.

III. Off-Line Policies Based on Full CSI and EAI

In this section, we propose off-line optimal and low-complexity sub-optimal policies that full CSI and EAI are assumed to be known at the BS.

A. Off-Line Optimal Policy

In this subsection, we first recast problem (5) in the form of GLFP using the mathematical preliminaries provided in Appendix A in order to propose our off-line optimal policy. Following [22], an GLFP can be written as below

$$\max_{\boldsymbol{x}}\ \Phi\left(\frac{f_1(\boldsymbol{x})[1]}{g_1(\boldsymbol{x})[1]},\cdots,\frac{f_M(\boldsymbol{x})[K+1]}{g_M(\boldsymbol{x})[K+1]}\right),\ \text{s.t }\boldsymbol{x}\in\psi,\tag{6}$$

where ψ is a nonempty polytope, $f_m(\boldsymbol{x})[i],g_m(\boldsymbol{x})[i]:\mathbb{R}^N\to\mathbb{R}$ for $m\in\mathcal{M}$, $i\in\mathcal{K}$ are linear functions, and $\Phi:\mathbb{R}_+^{M(K+1)}\to\mathbb{R}$ is an increasing function.

By defining $f_m[i]:=\sum_{j=1}^{M}|\boldsymbol{h}_m^H[i]\boldsymbol{w}_j[i]|^2+\sigma^2$ and $g_m[i]=\sum_{j\neq m}^{M}|\boldsymbol{h}_m^H[i]\boldsymbol{w}_j[i]|^2+\sigma^2$ and the fact that the logarithm is an one-to-one and increasing function, we can write problem (5) as

$$\begin{aligned}\max_{\substack{\boldsymbol{w}_1[i],\cdot,\boldsymbol{w}_M[i]\\ \text{for } i=\{1,\cdots,K+1\}}}\quad&\frac{1}{(K+1)M}\prod_{i=1}^{K+1}\prod_{m=1}^{M}\frac{f_m[i]}{g_m[i]},\\ &\text{s.t. }(3),\ (4),\text{ and (5a).}\end{aligned}\tag{7}$$

Let us assume that the feasible set of problem (5) contains $\psi=\omega\cap\mathcal{X}$ in which ω is a normal set constructed by (3) and $\mathcal{X}$ is an inverse normal set built by (4) and (5a). Note that normal and inverse normal sets are defined in Appendix A. Moreover, the objective value can be written as $\Phi(\boldsymbol{z})=\frac{1}{K+1}\prod_{i=1}^{K+1}\prod_{m=1}^{M}z_m[i]$ which is a product of linear fractional functions, hence it is an increasing function. Accordingly, we can conclude that the optimization problem belongs to the class of GLFP and write

$$\mathrm{OP}^1:\max_{\boldsymbol{z}}\ \frac{1}{K+1}\prod_{i=1}^{K+1}\prod_{m=1}^{M}z_m[i],\ \text{s.t. }\boldsymbol{z}\in\mathcal{D},\tag{8}$$

in which $\mathcal{D}=\left\{\boldsymbol{z}\middle|0\leq z_m[i]\leq\frac{f_m[i]}{g_m[i]},\boldsymbol{w}_m[i]\in\psi,\forall i,m\right\}$ where is a set constructed by an infinite number of boxes with the vertex set $\left\{\boldsymbol{r}\middle|r_m[i]=\frac{f_m[i]}{g_m[i]},\boldsymbol{w}_m[i]\in\psi,\forall i,m\right\}$. Each element of $\boldsymbol{r}$ can be uniquely determined by the beamforming vectors in ψ. The functions $f_m[i]$ and $g_m[i]$ are positive and independent because of the term σ^2. Let us denote $\boldsymbol{z}^\star\in\mathbb{R}^{M(K+1)\times1}$ as the optimal solution of the above problem. Since the objective value of OP^1 is an increasing function, $\boldsymbol{z}^\star$ obtains at the upper bound of $\boldsymbol{z}$, i.e., $z_m^\star[i]=\frac{f_m^\star[i]}{g_m^\star[i]}$

Algorithm 1: The optimal solution of OP^1.

1: Set $\epsilon_1>0$, $t_1=1$ as the error tolerance level and the iteration step, respectively.
2: Initialize the polyblock P with the vertex $\boldsymbol{z}^1$ by setting its elements as $z_m[i]=\max_{m,i}\frac{f_m[i]}{g_m[i]}=1+\frac{\|\boldsymbol{h}_m[i]\|^2}{\sigma^2}$, for $i\in\mathcal{K},m\in\mathcal{M}$.
3: **Repeat**
4: Find the projection vector of the vertex $\boldsymbol{z}^{t_1}$ on the the set ω using Algorithm 2.
5: Construct $M(K+1)$ new vertices by replacing $\boldsymbol{z}^{t_1}$ with $\{\bar{\boldsymbol{z}}^{1,t_1},\cdots,\bar{\boldsymbol{z}}^{M(K+1),t_1}\}$, $\bar{z}^{j,t}=\boldsymbol{z}^{t_1}-(z_j^{t_1}-\pi_j^{\omega}(\boldsymbol{z}^{t_1}))\boldsymbol{e}^j$.
6: Remove the improper vertices using the technique provided after Proposition 2.
7: Obtain $\boldsymbol{z}^{t_1+1}$ that maximizes the objective value of OP^1 over the set $\mathcal{D}$ as $\boldsymbol{z}_{t_1}^*=\operatorname{argmax}\left\{\Phi(\boldsymbol{z})=\frac{1}{K+1}\prod_{i=1}^{K+1}\prod_{m=1}^{M}z_m[i]\middle|\boldsymbol{z}\in\mathcal{D}\right\}$. Set $\boldsymbol{z}^{t_1+1}=\boldsymbol{z}_{t_1}^\star$ and $t_1=t_1+1$.
8: **Until** $\frac{\|\boldsymbol{z}^{t_1}-\boldsymbol{\pi}^{\omega}(\boldsymbol{z}^{t_1})\|}{\|\boldsymbol{z}^{t_1}\|}\leq\epsilon_1$
Result: The optimal beamforming vectors $\boldsymbol{w}_m^\star[i]=\boldsymbol{w}_m^{t_1}[i],\ \forall i,m.$

$i \in \mathcal{K}, m \in \mathcal{M}$, where $f_m^\star[i]$ and $g_m^\star[i]$ are associated with the optimal beamforming vectors.

As it is proven in Appendix A, the maximum of an increasing function over an intersection of normal and inverse normal sets occurs at the upper boundary set of the normal set. The optimal solution $\boldsymbol{z}^\star$ is obtained at the boundary of ω, i.e., $\delta^+\omega$. Consequently, we can shrink the polyblock with the vertex set contained the set ψ as shown in Figs. 8 (b, c, d) in Appendix A.

Now, we present a novel algorithm using GLFP [22] to achieve an optimal policy for OP^1. Let us first assume that there are no battery overflow constraints and QoS requirements for the users. The algorithm is summarized as follows.

As the first step of the algorithm, we construct a polyblock P with the vertex set $\mathcal{T}$ where each element can be written as $z_m[i] = \max \frac{f_m[i]}{g_m[i]} = 1 + \frac{\|\boldsymbol{h}_m[i]\|^2}{\sigma^2}, \forall i \in \mathcal{K}, m \in \mathcal{M}$, which contains the feasible set of OP^1 without battery overflow constraints and QoS requirements, i.e., ω. By using Proposition 1, the maximum of the objective value of OP^1 is obtained at one of the proper vertices of $\mathcal{T}$, assuming $\boldsymbol{z}^1$. If $\boldsymbol{z}^1$ belongs to the feasible set ω, then $\boldsymbol{z}_1^\star = \boldsymbol{z}^1$, otherwise, we start shrinking the polyblock. Regarding Proposition 2, we are able to build the smaller polyblock P_1 that excludes $\boldsymbol{z}^1$ and still contains the feasible set ω. We can construct this smaller polyblock by replacing $\boldsymbol{z}^1$ with $M(K+1)$ new vertices, $\boldsymbol{z}^j = \boldsymbol{z} - (z_j - \pi_j^\omega(\boldsymbol{z}_1))\boldsymbol{e}^j$, where $\boldsymbol{e}^j$ is j-th standard vector of $\mathbb{R}^{M(k+1)}$, z_j and $\pi_j^\omega(\boldsymbol{z}_1)$ are j-th element of the vectors $\boldsymbol{z}$ and $\boldsymbol{\pi}^\omega(\boldsymbol{z}_1)$, respectively. It is worth noting that some of the vertices are improper which can be removed using the technique provided after Proposition 2 (see Fig. 8 (c)). Then, we solve the optimization problem in seven line of Algorithm 1 to obtain the solution $\boldsymbol{z}_{t_1}^\star$, where t_1 is the iteration step of Algorithm 1. We can iteratively repeat this procedure to obtain the optimal solution of OP^1. Indeed, we can construct a sequence of polyblock such that $\omega \subset \cdots \subset P_1 \subset P$. It is obvious that the objective value of OP^1 in each step of the procedure satisfies $\Phi(\boldsymbol{z}_1^\star) \geq \Phi(\boldsymbol{z}_2^\star) \geq \cdots \geq \Phi(\boldsymbol{z}^\star)$. The algorithm is stopped when $\frac{\|\boldsymbol{z}^{t_1} - \boldsymbol{\pi}^\omega(\boldsymbol{z}^{t_1})\|}{\|\boldsymbol{z}^{t_1}\|} \leq \epsilon_1$ where $\epsilon_1 > 0$ is a small constant that shows the error tolerance. The algorithm can be enhanced by considering battery overflow constraints and QoS requirements for the users as $\boldsymbol{z}_{t_1}^\star$ is selected from a smaller set. Note that this has no contradiction with the optimality or convergence of the proposed algorithm because the optimal solution is still obtained at the boundary set of ψ as proven in Section A (see Figs. 8 (b, c, d)). The details of the algorithm are summarized in Algorithm 1.

Implementing the third step of Algorithm 1 is challenging as $\delta^+\omega$ is not explicitly determined. More precisely, for solving $\boldsymbol{\pi}^\omega(\boldsymbol{z}) = \lambda \boldsymbol{z}$, we need to solve the following optimization problem

$$\begin{aligned}\lambda^{t_1} &= \max\{\alpha | \alpha \boldsymbol{z}^{t_1} \in \omega\} \\ &= \max\{\alpha | \alpha \leq \min_{i\in\mathcal{K}, m\in\mathcal{M}} \frac{f_m[i]}{z_m^{t_1}[i] g_m[i]}, \boldsymbol{w}_m[i] \in \psi, \forall i, m\} \\ &= \max_{\boldsymbol{w}_m[i]\in\psi, \forall i, m} \min_{i\in\mathcal{K}, m\in\mathcal{M}} \frac{f_m[i]}{z_m^{t_1}[i] g_m[i]}, \end{aligned} \tag{9}$$

Algorithm 2: The projection of $\boldsymbol{z}^{t_1}$ on the set ω.

1: Initialize $\boldsymbol{w}_m[i],\ \forall i, m$ randomly, and set $t_2 = 1$ as the iteration step.
2: **Repeat**
3: For given beamforming vectors, solve $\lambda^{t_2} = \min_{i\in\mathcal{K}, m\in\mathcal{M}} \frac{f_m[i]}{z_m^{t_1}[i] g_m[i]}$
4: For given λ^{t_2}, solve $\max_{\boldsymbol{w}_m[i]\in\psi, \forall i, m} \min_{i\in\mathcal{K}, m\in\mathcal{M}} (f_m[i] - \lambda^{t_2} z_m[i] g_m[i])$. Set $t_2 = t_2 + 1$.
6: **Until** $\max_{\boldsymbol{w}_m[i]\in\psi, \forall i, m} \min_{i\in\mathcal{K}, m\in\mathcal{M}} \left(f_m[i] - \lambda^{t_2} z_m[i] g_m[i]\right) \leq 0$
Result: The projection of $\boldsymbol{z}^{t_1}$ on the set ω.

where is a max-min problem which can be considered in the class of GLFP. We employ the Dinkelbach-type technique with a little change to solve this problem. More precisely, in the first step of the technique, we randomly initialize the beamforming vectors and set $t_2 = 1$ as the iteration step. Then, for given beamforming vectors, we solve $\lambda^{t_2} = \min_{i\in\mathcal{K}, m\in\mathcal{M}} \frac{f_m[i]}{z_m^{t_1}[i] g_m[i]}$. By using the obtained λ^{t_2}, we solve $\max_{\boldsymbol{w}_m[i]\in\psi, \forall i, m} \min(f_m[i] - \lambda^{t_2} z_m[i] g_m[i])$. The algorithm is stopped when $\max_{\boldsymbol{w}_m[i]\in\psi, \forall i, m} \min_{i\in\mathcal{K}, m\in\mathcal{M}} \left(f_m[i] - \lambda^{t_2} z_m[i] g_m[i]\right) \leq 0$ which ensures that the resulting resource allocation lies on the set $\delta^+\omega$. The details of the algorithm are shown in Algorithm 2 which can be solved by numerical solver such as CVX [25]. The convergence of Algorithm 2 can be straightforwardly proven using [26, Theorem 8.7] which is based on the Q-super linear convergence technique.

***Theorem** 1:* Algorithm 1 is convergent to the global optimal solution of OP^1.

Proof: See Appendix B for the proof.

It is worth noting that the above approach obtains the optimal policy as Algorithm 2 ensures that the solution of resource allocation lies on the feasible set of OP^1.

B. Off-Line Low-Complexity Sub-Optimal Policy

In this subsection, we provide an off-line low-complexity sub-optimal policy for problem (5). The approach is based on the successive convex approximation and block coordinate descent techniques. We first show that the non-convex objective function and QoS requirements of problem (5) can be approximated by convex functions using their first-order Taylor expansions. Then, using the block coordinate descent technique, we propose an algorithm to tighten the obtained solution. Let us first define $\boldsymbol{W}_m[i] = \boldsymbol{w}_m^H[i]\boldsymbol{w}_m[i], \boldsymbol{H}_m[i] = \boldsymbol{h}_m^H[i]\boldsymbol{h}_m[i]$. Then, by assuming $\mathrm{rank}(\boldsymbol{W}_m[i]) = 1, \forall i, m$, we

can rewrite problem (5) as below

$$\max_{\substack{\boldsymbol{W}_m[i],\\ \forall i,m}} \frac{1}{(K+1)M}\sum_{i=1}^{K+1}\sum_{m=1}^{M}\left[\log_2\left(\sum_{j=1}^{M}\mathrm{tr}(\boldsymbol{H}_m[i]\boldsymbol{W}_j[i])+\sigma^2\right) - G\right]$$

$$\text{s.t. } (3),\ (4),$$

$$\log_2\left(\sum_{j=1}^{M}\mathrm{tr}(\boldsymbol{H}_m[i]\boldsymbol{W}_j[i])+\sigma^2\right) - G \geq R^{\mathrm{q}}, \forall\ m,i, \tag{10a}$$

$$\mathrm{rank}(\boldsymbol{W}_m[i]) = 1,\ \forall i,m, \tag{10b}$$

where $G := \log_2\left(\sum_{j\neq m}^{M}\mathrm{tr}(\boldsymbol{H}_m[i]\boldsymbol{W}_j[i])+\sigma^2\right)$.

Note that the objective value and constraint (10a) of problem (10) are still non-convex because they are the difference of two convex functions. However, we use the successive convex approximation approach to obtain a locally optimal solution for problem (10). In particular, by using the first-order Taylor expansion for any arbitrary convex function $f(\boldsymbol{t})$ at the local point $\tilde{\boldsymbol{t}}$, there exists a lower bound on $f(\boldsymbol{t})$ as below [19] $f(\boldsymbol{t}) \geq f(\tilde{\boldsymbol{t}}) + \nabla_{\boldsymbol{t}} f(\tilde{\boldsymbol{t}})^T(\boldsymbol{t}-\tilde{\boldsymbol{t}})$. Consequently, G at the local point $\tilde{\boldsymbol{W}}_m[i]$ can be bounded by

$$G \geq \log_2\left(\sum_{j\neq m}^{M}\mathrm{tr}(\boldsymbol{H}_m[i]\tilde{\boldsymbol{W}}_j[i])+\sigma^2\right) + \sum_{j\neq m}^{M}\mathrm{tr}\left(\frac{\boldsymbol{H}_m[i](\boldsymbol{W}_j[i]-\tilde{\boldsymbol{W}}_j[i])}{(\sum_{r\neq m}\mathrm{tr}(\boldsymbol{H}_m[i]\tilde{\boldsymbol{W}}_r[i])+\sigma^2)\ln 2}\right), \tag{11}$$

where is a summation of convex and linear functions, hence convex. By dropping the rank constraints, we can recast problem (10) as

$$\mathrm{OP}^2: \max_{\substack{\boldsymbol{W}_m[i],\\ \boldsymbol{R}[i],\forall i,m}} \frac{1}{(K+1)M}\sum_{i=1}^{K+1}\sum_{m=1}^{M}\left[\log_2\left(\sum_{j=1}^{M}\mathrm{tr}(\boldsymbol{H}_m[i]\boldsymbol{W}_j[i])+\sigma^2\right) - \log_2\left(\sum_{j\neq m}^{M}\mathrm{tr}(\boldsymbol{H}_m[i]\tilde{\boldsymbol{W}}_j[i])+\sigma^2\right) - \sum_{j\neq m}^{M}\mathrm{tr}\left(\frac{\boldsymbol{H}_m[i](\boldsymbol{W}_j[i]-\tilde{\boldsymbol{W}}_j[i])}{(\sum_{r\neq m}\mathrm{tr}(\boldsymbol{H}_m[i]\tilde{\boldsymbol{W}}_r[i])+\sigma^2)\ln 2}\right)\right],$$

$$\text{s.t. } (3),\ (4),$$

$$\log_2\left(\sum_{j=1}^{M}\mathrm{tr}(\boldsymbol{H}_m[i]\boldsymbol{W}_j[i])+\sigma^2\right) - \log_2\left(\sum_{j\neq m}^{M}\mathrm{tr}(\boldsymbol{H}_m[i]\tilde{\boldsymbol{W}}_j[i])+\sigma^2\right) - \sum_{j\neq m}^{M}\mathrm{tr}\left(\frac{\boldsymbol{H}_m[i](\boldsymbol{W}_j[i]-\tilde{\boldsymbol{W}}_j[i])}{(\sum_{r\neq m}\mathrm{tr}(\boldsymbol{H}_m[i]\tilde{\boldsymbol{W}}_r[i])+\sigma^2)\ln 2}\right) \geq R^q,$$

$$\boldsymbol{R}[i] \geq \sum_{j=1}^{M}\boldsymbol{W}_j[i], \forall\ m,i. \tag{12a}$$

Algorithm 3: The block coordinate descent technique for the low-complexity sub-optimal policy of OP^2.

1: Initialize $\boldsymbol{W}_m^1[i], \forall i,m$, and set $t_3 = 1$ and $\epsilon_3 \ll 1$ as the iteration step and error tolerance, respectively.
2: **Repeat**
3: For given $\boldsymbol{W}_m^{t_3}[i]$, solve (12) and store the optimal solution of $\hat{\boldsymbol{W}}_m[i]$ in $\boldsymbol{W}_m^{t_3+1}[i]$, i.e., $\boldsymbol{W}_m^{t_3+1}[i] \longleftarrow \hat{\boldsymbol{W}}_m[i]$. Set $t_3 = t_3+1$.
5: **Until** $\frac{\|\boldsymbol{W}_m^{t_3}[i]-\boldsymbol{W}_m^{t_3-1}[i]\|}{\|\boldsymbol{W}_m^{t_3-1}[i]\|} \leq \epsilon_3, \forall i,m$
Result: The final beamforming matrices $\boldsymbol{W}_m^{\star}[i] = \boldsymbol{W}_m^{t_3}[i]$. If the solution is not the rank-one, one use the procedure explained in Section III-B.

The feasible set of problem (12) serves as a subset for the feasible set of problem (10) because of the lower bounds derived in (11) and using the first-order Taylor expansion. Consequently, the objective value of problem (12) is always less than its counterpart in problem (10).

Now, we deal with the non-convex rank constraints in (10b). We relaxed the rank constraints of problem (10) and expressed problem OP^2, which is convex, hence it can be efficiently solved using CVX. Let $\boldsymbol{W}_m^{\star}[i]$ and $\boldsymbol{R}^{\star}[i]$ be the optimal solution of OP^2. If $\mathrm{rank}(\boldsymbol{W}_m^{\star}[i]) = 1$, the solution is tight, otherwise, one might need to construct the rank-one solution of OP^2 using the Gaussian randomization technique proposed in [27]. However, in the following, we show that one always can find a rank-one solution for OP^2.

Let us first construct a new solution $\hat{\boldsymbol{W}}_m[i]$ such that

$$\hat{\boldsymbol{w}}_m[i] = (\boldsymbol{h}_m^H[i]\boldsymbol{W}_m^{\star}[i]\boldsymbol{h}_m[i])^{-\frac{1}{2}}\boldsymbol{W}_m^{\star}[i]\boldsymbol{h}_m[i],$$
$$\hat{\boldsymbol{W}}_m[i] = \hat{\boldsymbol{w}}_m[i]\hat{\boldsymbol{w}}_m^H[i]. \tag{13}$$

Now, we show that $\hat{\boldsymbol{W}}_m[i]$ is the optimal solution for OP^2. To do this, for any vector $\boldsymbol{v}$, we have

$$\boldsymbol{v}^H(\boldsymbol{W}_m^{\star}[i]-\hat{\boldsymbol{W}}_m[i]) = \boldsymbol{v}^H\boldsymbol{W}_m^{\star}[i]\boldsymbol{v} - (\boldsymbol{h}_m^H[i]\boldsymbol{W}_m^{\star}[i]\boldsymbol{h}_m[i])^{-1}|\boldsymbol{v}^H\boldsymbol{W}_m^{\star}[i]\boldsymbol{h}_m[i]|^2. \tag{14}$$

Regarding the Cauchy-Schwarz inequality, one can write

$$\begin{aligned}|\boldsymbol{v}^H\boldsymbol{W}_m^{\star}[i]\boldsymbol{h}_m[i]|^2 &= |\boldsymbol{v}^H\boldsymbol{w}_m^{\star}[i]\boldsymbol{w}_m^H[i]\boldsymbol{v}|^2\\ &\leq |\boldsymbol{v}^H\boldsymbol{w}_m^H[i]|^2|\boldsymbol{h}_m^H[i]\boldsymbol{w}_m^H[i]|^2\\ &= (\boldsymbol{v}^H\boldsymbol{W}_m^{\star}[i]\boldsymbol{v})(\boldsymbol{h}_m^H[i]\boldsymbol{W}_m^{\star}[i]\boldsymbol{h}_m[i]).\end{aligned} \tag{15}$$

Hence,

$$\boldsymbol{v}^H(\boldsymbol{W}_m^{\star}[i]-\hat{\boldsymbol{W}}_m[i]) \geq 0, \forall m. \tag{16}$$

Consequently, $\boldsymbol{W}_m^{\star}[i]-\hat{\boldsymbol{W}}_m[i] \succeq 0$ and $\hat{\boldsymbol{R}}[i] \succeq \sum_{j=1}^{M}\boldsymbol{W}_j^{\star}[i]$.

Now, it is required to show that the objective value of OP^2 does not change with this new solution. To do so, by using (13), we can write

$$\begin{aligned}\mathrm{tr}(\boldsymbol{H}_m[i]\hat{\boldsymbol{W}}_m[i]) &= \boldsymbol{h}_m^H[i]\hat{\boldsymbol{W}}_m[i]\boldsymbol{h}_m[i]\\ &= \boldsymbol{h}_m^H[i]\hat{\boldsymbol{w}}_m[i]\hat{\boldsymbol{w}}_m^H[i]\boldsymbol{h}_m[i]\\ &= \boldsymbol{h}_m^H[i]\boldsymbol{W}_m^{\star}[i]\boldsymbol{h}_m[i],\ \forall m,\end{aligned} \tag{17}$$

then, the first and third terms of the objective value of OP^2 can be written as

$$\begin{aligned}
&\log_2\left(\sum_{j=1}^{M}\mathrm{tr}(\boldsymbol{H}_m[i]\hat{\boldsymbol{W}}_j[i])+\sigma^2\right)\\
&=\log_2\left(\sum_{j=1}^{M}\mathrm{tr}(\boldsymbol{H}_m[i]\boldsymbol{W}_j^{\star}[i])+\sigma^2\right),\\
&\sum_{j\neq m}^{M}\mathrm{tr}\left(\frac{\boldsymbol{H}_m[i](\hat{\boldsymbol{W}}_j[i]-\tilde{\boldsymbol{W}}_j[i])}{(\sum_{r\neq m}\mathrm{tr}(\boldsymbol{H}_m[i]\tilde{\boldsymbol{W}}_r[i])+\sigma^2)\ln 2}\right)\\
&=\sum_{j\neq m}^{M}\mathrm{tr}\left(\frac{\boldsymbol{H}_m[i](\boldsymbol{W}_j^{\star}[i]-\tilde{\boldsymbol{W}}_j[i])}{(\sum_{r\neq m}\mathrm{tr}(\boldsymbol{H}_m[i]\tilde{\boldsymbol{W}}_r[i])+\sigma^2)\ln 2}\right),
\end{aligned}\tag{18}$$

which means that the objective value remains the same.

Here, the lower bounds employed in problem (12) are then tightened using the block coordinate descent technique summarized in Algorithm 3. The convergence of Algorithm 3 is presented in the following theorem.

***Theorem** 2:* Algorithm 3 is convergent.

Proof: See Appendix C for the proof.

Numerical evaluations in Section VI also reveal that proposed Algorithm 3 converges quickly.

IV. On-Line Policies Based on Statistical CSI and EAI

In this section, motivated by the off-line policies, we propose on-line optimal and low-complexity sub-optimal policies, where only statistical CSI and EAI are available at the BS. In practice, the instantaneous channel states in frequency division duplex and time division duplex can be calculated by feedback and channel reciprocity, respectively [14]. Moreover, information regarding the current energy arrivals are known at the BS only after being collected. Consequently, the BS is not aware of future channel states and energy arrivals. In case of imperfect CSI and EAI, however, it is possible to adopt our approach for the average CSI and EAI, which are available by a long term measurement. To do so, we can first obtain the number of the events using statistical information regarding the energy CSI and EAI. As number of events is Poisson process with rate $\lambda_C+\lambda_E$, the expected number of events in the interval $(0,T]$ is $\bar{K}=(\lambda_C+\lambda_E)T$. Consequently, the expected length of each time slot can be written as $\bar{L}=\frac{T}{\bar{K}}$. Moreover, the expected energy value for i-th time slot is $\bar{E}[i]=\frac{E_{\min}[i]+E_{\max}[i]}{2}$. Then, by assuming that the BS is currently working at the i_0-th time slot, we can write the optimization problem for the i_0-th and future time slots as

$$\max_{\substack{\boldsymbol{w}_1[i],\cdots,\boldsymbol{w}_M[i]\\ \text{for } i=\{1,\cdots,K+1\}}}\ \frac{1}{(\bar{K}+1)M}\sum_{m=1}^{M}\sum_{i=i_0}^{\bar{K}+1}\bar{R}_m[i]$$

$$\text{s.t.}\sum_{i=i_0}^{k}\left(\sum_{m=1}^{M}\|\boldsymbol{w}_m[i]\|^2\right)\bar{L}\leq\sum_{i=i_0}^{k}\bar{E}[i],\tag{19a}$$

$$\sum_{i=i_0}^{k}\left(\sum_{m=1}^{M}\|\boldsymbol{w}_m[i]\|^2\right)\bar{L}\geq\sum_{i=i_0}^{k}\bar{E}[i]-E_{\max},\tag{19b}$$

$$\bar{R}_m[i]\geq R^{\mathrm{q}},\ \forall\ m,i\in\{i_0,\cdots,\bar{K}+1\},\tag{19c}$$

where $\bar{R}_m[i]=B\log_2\left(1+\bar{\gamma}_m[i]\right)$ and $\bar{\gamma}_m[i]=\frac{|\bar{\boldsymbol{h}}_m^H[i]\boldsymbol{w}_m[i]|^2}{\sum_{j\neq m}^{M}|\bar{\boldsymbol{h}}_m^H[i]\boldsymbol{w}_j[i]|^2+\sigma^2}$, in which $\bar{\boldsymbol{h}}_m[i]$ is the expected value of channel at the $i-$th time slot for the $m-$th user. The objective value of problem (19) maximizes the achievable system throughput for the current time slot i_0 and future time slots $i_0+1\leq i\leq\bar{K}+1$. Constraints (19a) and (19b) ensure energy casualty and battery overflow constraints for the current and future time slots, respectively. Constraint (19c) bounds the expected achievable data rate in current and future time slots. The objective value of problem (19) and constraint (19c) are non-convex, thus solving the optimization problem in (19) introduces non-convexity. Nevertheless, inspired by the derived off-line policies, in the following, we propose on-line policies.

A. On-Line Optimal Policy

In this subsection, we develop an on-line optimal policy for the optimization problem in (19). To utilize the GLFP approach, we rewrite problem (19) as below

$$\max_{\substack{\boldsymbol{w}_1[i],\cdots,\boldsymbol{w}_M[i]\\ \text{for } i=\{i_0,\cdots,K+1\}}}\ \frac{1}{\bar{K}+1}\prod_{i=i_0}^{\bar{K}+1}\prod_{m=1}^{M}\frac{f_m[i]}{g_m[i]},\tag{20}$$

$$\text{s.t.}\quad\text{(19a), (19b), and (19c)},\tag{21}$$

where $f_m[i]:=\sum_{j=1}^{M}|\bar{\boldsymbol{h}}_m^H[i]\boldsymbol{w}_j[i]|^2+\sigma^2$ and $g_m[i]=\sum_{j=1}^{M}|\bar{\boldsymbol{h}}_m^H[i]\boldsymbol{w}_j[i]|^2+\sigma^2$. Note that $\psi=\omega\cap\mathcal{X}$ such that the feasible set ω is constructed by constraint (19a). In addition, the feasible set $\mathcal{X}$ is constructed by constraints and (19b) and (19c). Similar to the off-line optimal policy, we can write

$$\mathrm{OP}^3:\max_{\boldsymbol{z}}\ \frac{1}{(\bar{K}+1)M}\prod_{i=i_0}^{\bar{K}+1}\prod_{m=1}^{M}z_m[i],\ \text{s.t. }\boldsymbol{z}\in\psi,\tag{22}$$

where $\mathcal{D}=\left\{\boldsymbol{z}\middle|0\leq z_m[i]\leq\frac{f_m[i]}{g_m[i]},\boldsymbol{w}_m[i]\in\psi,\forall i\in\{i_0,\cdots,\bar{K}\},m\right\}$ with the vertex set $\left\{\boldsymbol{r}\middle|r_m[i]=\frac{f_m[i]}{g_m[i]},\boldsymbol{w}_m[i]\in\psi,\forall i\in\{i_0,\cdots,\bar{K}\},m\right\}$. Following Subsection III-A, we implement Algorithm 1 for optimization problem OP^3 and obtain the on-line optimal policy. In Section VI, we experimentally compare the performance of the proposed off-line and on-line optimal policies.

TABLE I: The total computational complexity of the proposed policies.

Policies:	The total computational complexity:
The off-line optimal policy	$t_1(MN_tK)^2 + t_1t_2\mathcal{O}((MN_tK)^{3.6})$.
The off-line low-complexity sub-optimal policy	$t_3\mathcal{O}\big((MN_tK)^{3.6}\big)$.
The on-line optimal policy	$\bar{t}_1(MN_t\bar{K})^2 + \bar{t}_1\bar{t}_2\mathcal{O}((MN_t\bar{K})^{3.6})$.
The on-line low-complexity sub-optimal policy	$\bar{t}_3\mathcal{O}\big((MN_t\bar{K})^{3.6}\big)$.

B. On-Line Low-Complexity Sub-Optimal Policy

Here, we study an on-line low-complexity sub-optimal policy which is based on the successive optimization and block coordinate descent techniques. By defining $\bar{\boldsymbol{H}}_m[i] = \bar{\boldsymbol{h}}_m^H[i]\bar{\boldsymbol{h}}_m[i]$ and dropping the rank constraints for the beamforming matrices, we can rewrite problem (19) as below

OP^4 :

$$\max_{\substack{\boldsymbol{W}_m[i],\\ \boldsymbol{R}[i]\forall i,m}} \frac{1}{(\bar{K}+1)M}\sum_{i=i_0}^{\bar{K}+1}\sum_{m=1}^{M}\Bigg[\log_2\Bigg(\sum_{j=1}^{M}\mathrm{tr}(\bar{\boldsymbol{H}}_m[i]\boldsymbol{W}_j[i])+\sigma^2\Bigg)$$
$$-\log_2\Bigg(\sum_{j\neq m}^{M}\mathrm{tr}(\bar{\boldsymbol{H}}_m[i]\tilde{\boldsymbol{W}}_j[i])+\sigma^2\Bigg)$$
$$-\sum_{j\neq m}^{M}\mathrm{tr}\Bigg(\frac{\bar{\boldsymbol{H}}_m[i](\boldsymbol{W}_j[i]-\tilde{\boldsymbol{W}}_j[i])}{(\sum_{r\neq m}\bar{\boldsymbol{H}}_m[i]\tilde{\boldsymbol{W}}_r[i])+\sigma^2)\ln 2}\Bigg)\Bigg],$$
s.t. (19a) and (19b),
$$\log_2\Bigg(\sum_{j=1}^{M}\mathrm{tr}(\bar{\boldsymbol{H}}_m[i]\boldsymbol{W}_j[i])+\sigma^2\Bigg)$$
$$-\log_2\Bigg(\sum_{j\neq m}^{M}\mathrm{tr}(\bar{\boldsymbol{H}}_m[i]\tilde{\boldsymbol{W}}_j[i])+\sigma^2\Bigg)$$
$$-\sum_{j\neq m}^{M}\mathrm{tr}\Bigg(\frac{\bar{\boldsymbol{H}}_m[i](\boldsymbol{W}_j[i]-\tilde{\boldsymbol{W}}_j[i])}{(\sum_{r\neq m}\mathrm{tr}(\bar{\boldsymbol{H}}_m[i]\tilde{\boldsymbol{W}}_r[i])+\sigma^2)\ln 2}\Bigg)\geq R^q,$$
$$\boldsymbol{R}[i]\succeq\sum_{j=1}^{M}\boldsymbol{W}_j[i],\forall\ m,i\in\{i_0,\cdots,\bar{K}+1\},\tag{23a}$$

at the local point $\tilde{\boldsymbol{W}}_m[i],\ \forall i,m$. OP^4 is convex and can be solved efficiently via CVX. We then apply Algorithm 3 in Subsection III-B to achieve the on-line low-complexity sub-optimal policy for OP^4. We investigate the performance of the proposed for the off-line and on-line low-complexity sub-optimal policies in Section VI.

V. COMPUTATIONAL COMPLEXITY ANALYSIS

The aim of this section is to investigate the total computational costs of the proposed resource allocation policies. It is worth mentioning that in Algorithm 1, some of the vertices are improper, which we are not able to determine in advance, thus we assume that none of them is improper and obtain the upper bound on the computational complexity for the off-line and on-line optimal policies. On the other hand, all approaches are based on convex optimizations which we need to implement them with numerical convex solvers such as CVX. The interior point method with the Newton step typically employed to solve the convex optimization imposes a complexity on the order of $\mathcal{O}\big((E+F)^{1.6}E^2\big)$ operations, where E and F are the number of variables and constraints in the optimization problem [19].

To determine the computational complexity of the off-line optimal policy, let us first define t_1, t_2 as the numbers of iterations until the convergence of Algorithms 1 and 2, respectively. In the second step of Algorithm 1, $MN_t(K+1)$ multiplications, $MN_t(K+1)$ divisions, and $MN_t(K+1)$ summations are needed, hence the computational complexity is $3MN_t(K+1)$. In the fourth step, we need to run Algorithm 2 to find $\boldsymbol{\pi}^\omega(\boldsymbol{z}^t)$. In the third step of Algorithm 2, we need to calculate $MN_t(K+1)$ multiplications and $MN_t(K+1)$ divisions, thus the complexity is $2MN_t(K+1)$. In the fourth step of Algorithm 2, an optimization problem with $MN_t(K+1)$ variables and $M(K+1)+2K+1$ constraints are necessary to implement, therefore the computational complexity follows $\mathcal{O}\big(((MN_t+M)(K+1)+2K+1)^{1.6}(MN_t(K+1))^2\big)$. Consequently, the overall complexity of Algorithm 2 until convergence is approximately $t_2\mathcal{O}\big((MN_tK)^{3.6}\big)$. One subtraction and multiplication are needed to construct each vertex in the fifth step of Algorithm 1, therefore, the complexity is $2MN_t(K+1)$. The sixth step of Algorithm 1 implies $MN_t(K+1)$ multiplications for each vertex and $MN_t(K+1)$ comparisons, then the complexity is $(MN_t(K+1))^2 + MN_t(K+1)$. Overall, the computational complexity of the off-line optimal policy until convergence is approximately

$$t_1(MN_tK)^2 + t_1t_2\mathcal{O}((MN_tK)^{3.6}).\tag{24}$$

As for each iteration of Algorithm 1 we need to map a vertex on the feasible set, implementing Algorithm 2, the dominant term of the computational complexity of Algorithm 1 belongs to this part.

For the low-complexity sub-optimal off-line policy, we need to implement Algorithm 3. For each step of Algorithm 3, the optimization problem in (12) is solved with $(MN_t+1)(K+1)$ variables $(M+1)(K+1)+2K+1$ constraints. By defining t_3 as the number of iterations until the convergence of Algorithm 3, the overall computational complexity of the low-complexity

This article has been accepted for publication in IEEE Transactions on Communications. This is the author's version which has not been fully edited and content may change prior to final publication. Citation information: DOI 10.1109/TCOMM.2022.3215997

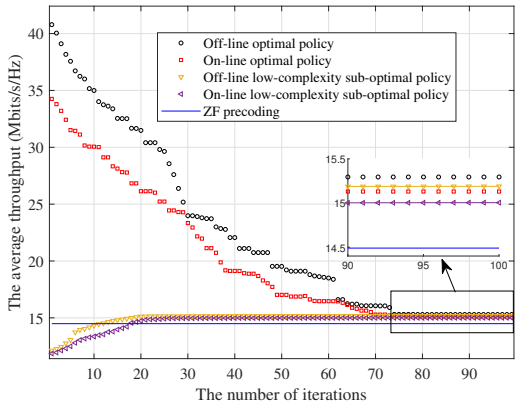

Fig. 3: The convergence behavior of the proposed policies for $E_{\max} = 1$ J, $E[0] = 1$ J, $E^{\max} = 1$ J, $\lambda_C = 1$ 1/s and $\lambda_E = 1$ J/s, and $N_t = M = 3$.

sub-optimal off-line policy approximately follows

$$t_3 \mathcal{O}\big((MN_tK)^{3.6}\big). \tag{25}$$

From the complexity derivations, it is obvious that obtaining the low-complexity sub-optimal policy, Algorithm 3, is faster than the optimal solution, Algorithm 1. We show this experimentally in Section VI. Note that we ignore the complexity of building the rank-one solution if it is necessary.

The last but not the least, the computational complexity of the on-line optimal and low-complexity sub-optimal policies can be approximately written as

$$\bar{t}_1 (MN_t\bar{K})^2 + \bar{t}_1\bar{t}_2 \mathcal{O}((MN_t\bar{K})^{3.6}). \tag{26}$$

and

$$\bar{t}_3 \mathcal{O}\big((MN_t\bar{K})^{3.6}\big), \tag{27}$$

by setting $i_0 = 1$ in (19), respectively, where $\bar{t}_1, \bar{t}_2,$ and $\bar{t}_3$ are the number of iteration in Algorithms 1, 2, and 3.

VI. Numerical Experiments

In this section, we evaluate the performance of the proposed approaches via Monte Carlo simulations. We assume that the bandwidth and noise power spectral density are $B = 1$ MHz and $N_0 = 10^{-13}$ W/Hz, respectively [14]. In addition, we use a Rayleigh channel model with complex normal variables with mean and variance $\mu_c = 5 \times 10^{-5}$ and $\sigma_c^2 = 10^{-10}$, respectively [15]. The number of BS antennas will be specified in each simulation. We set $\epsilon_1 = \epsilon_3 = 10^{-4}$ in the proposed algorithms. Without loss of generality, we assume that $T = [0, 5)$, $R^q = 0.5$ Mbits/s/Hz, $E^{\max} = E_{\max}[i]$ and $E_{\min}[i] = 0$ for all i [14]. We compare the performance of the proposed polices with the off-line and on-line ZF precoding [15] as a benchmark. To have a fair comparison, we use use the same CSI and EAI for all the methods.

A. Convergence Behavior of the Proposed Policies

In this subsection, we study the convergence behavior of the proposed policies. To do so, we assume that $\lambda_C = 1$ 1/s, $\lambda_E = 1$ J/s and $E^{\max} = 1$ J. We set $N_t = M = 3$ $E[0] = 1$ J and $E_{\max} = 1$ J. Also, full CSI and EAI are available at the BS for obtaining off-line policies. We consider $t_E = [0.29, 1.4, 2.18, 3.57, 4.22]^T$ s $t_C = [2.8, 4.48]^T$ s. Thus, $\boldsymbol{\ell} = [0.29, 1.11, 0.78, 0.62, 0.77, 0.65, 0.26, 0.52]^T$ s. Energies arrive in amounts $\boldsymbol{E} = [0.14, 0.52, 0.49, 0.93, 0.84]^T$ J. Hence, $\boldsymbol{E}_{in} = [1, 0, 0.14, 0.52, 0.49, 0, 0.93, 0.84, 0]^T$ J. Note that in order to provide fair comparison between the on-line and off-line policies, we set $i_0 = 1$ in (19). Fig. 3 shows the average throughput versus the number of iterations for the proposed policies. From this figure, one can note that both optimal and low-complexity sub-optimal policies converge to almost same average throughput, which outperforms the ZF precoding. Algorithm 3 converges quickly while more iterations are needed in order to implement Algorithm 1 for the optimal policy. It is observed from this figure that the off-line optimal policies serve as an upper bound for other polices. In addition, the optimal policies can achieve better performance than low-complexity sub-optimal policies.

B. The Effects of Battery Overflow Constraints

In this subsection, we investigate the effects of battery size in (4) on the average system throughput. Intuitively, it is beneficial to have a battery with large size to store more harvested energy. Therefore, it is expected by implementing the proposed optimization in (5) with a large battery size, better performance can be achieved.

For this simulation, we assume that $N_t = M = 3$, energies arrive at every second in amounts $\boldsymbol{E} = [1, 1, 1, 1]^T$ J and the channel gains change at every second. The available energy in the battery at 0 is assumed to be $E[0] = 1$ J. Hence, $\boldsymbol{E}_{in} = [1, 1, 1, 1, 1]^T$ J and $\boldsymbol{\ell} = [1, 1, 1, 1, 1]^T$. For better illustration, we only implement the off-line low-complexity sub-optimal policy in this simulation. Assuming 4 events happen during the transmission interval, we adapt our proposed resource allocation policy 5 times.

In Fig. 4, we plot the average throughput for the off-line low-complexity policy when the size of the battery is changed. The consumed energy by the system in each time slot is plotted in black lines at the middle of each time slot in Figs. 4 (a) and (b). In addition, the blue line shows the upper bound for the consumed energy by the system as its associated with the energy casualty constraints in (3). Also, the battery overflow constraints in (4) are depicted by the red line. Figs. 4 (a) and (b) are corresponding to the case when $E_{\max} = 1, 0.25$ J, respectively. Indeed, these constraints provide a situation in which most of the arrival energies used for communication purposes. From Fig. 4 (c), it is observed that better performance in terms of the average throughput up to 0.14 Mbits/s/Hz is obtained when a battery with size 1 J is implemented.

C. The Average System Throughput Versus the Rate of Energy Arrivals

We examine the average throughput versus the rate of energy arrivals during the transmission interval with $E_{\max} = 1$ J, $E[0] = 1$ J, $N_t = M = 3$, $\lambda_E = 1$ J/s, $\lambda_C = 1$ 1/s

This article has been accepted for publication in IEEE Transactions on Communications. This is the author's version which has not been fully edited and content may change prior to final publication. Citation information: DOI 10.1109/TCOMM.2022.3215997

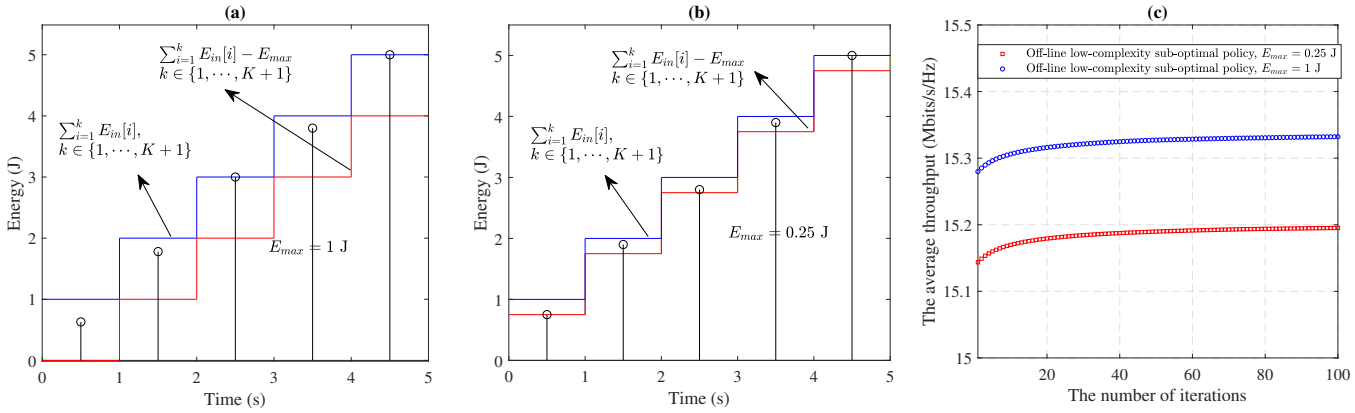

Fig. 4: Figs. 4 (a) and (b) show the consumed energy for $E_{\max} = 1$ J and $E_{\max} = 0.25$ J, respectively, for the off-line low-complexity sub-optimal policy. Fig. 4 (c) compares the average throughput for these battery sizes.

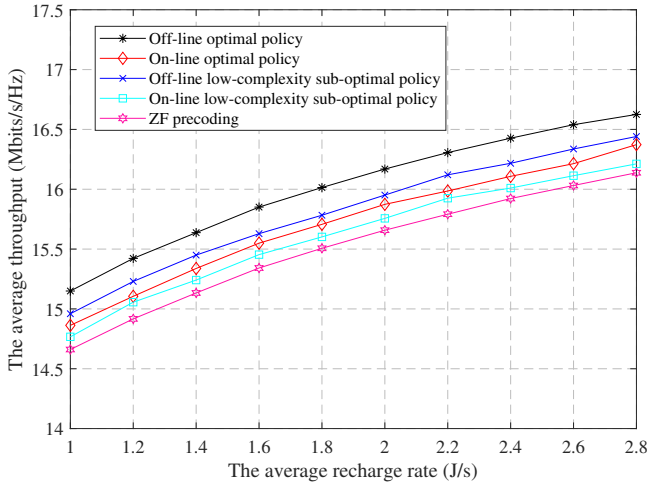

Fig. 5: The average system throughput versus the average recharge rate over 100 trials for $E_{\max} = 1$ J, $E[0] = 1$ J, $\lambda_C = 1$ 1/s, and $N_t = M = 3$.

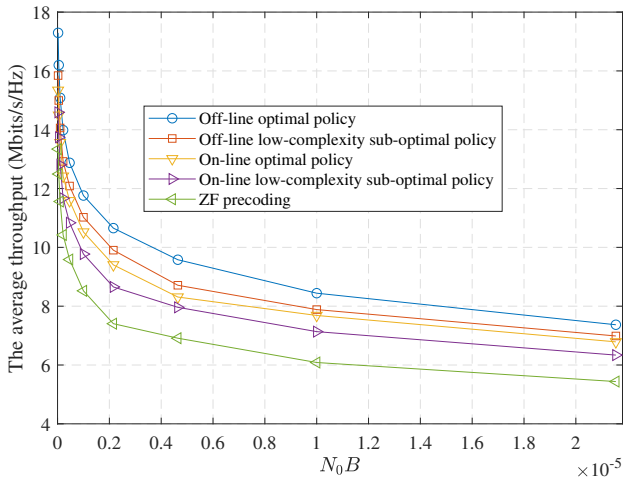

Fig. 6: A comparison among the proposed policies in terms of the average throughput versus the power of AWGN over 100 trials for $\lambda_C = 1$ 1/s, $\lambda_E = 1$ J/s, $N_t = M = 3$, $E^{\max} = 1$ J, $E[0] = 1$ J, and $E_{\max} = 1$ J.

as depicted in Fig. 5. Each point of simulations is obtained through 100 trials. We observe that the average throughout for all proposed policies is an increasing function of energy arrivals rate. The off-line scenario outperforms the on-line scenario as full CSI and EAI are assumed to be available at the BS. It is also observed that the optimal solution obtains better performance than the low-complexity sub-optimal policy. In addition, the proposed policies which directly solve the beamforming problem outperform the ZF precoding.

D. The Average Throughput Versus the Power of AWGN

In this subsection, we examine the performance of the proposed approaches in terms of the average throughput versus the power of AWGN as shown in Fig. 6. Each point of simulation is achieved through 100 trials. For this simulation, we set $\lambda_C = 1$ 1/s, $\lambda_E = 1$ J/s, $N_t = M = 3$, $E^{\max} = 1$ J, $E[0] = 1$ J, $E_{\max} = 1$ J. It is observed from Figs. 6 (a) and (b) that by increasing the power of AWGN, the average throughput for the proposed policies decreases. In addition, the performance achieved by the proposed off-line policies is better than the on-line policies. In addition, the proposed policies outperform the ZF precoding.

E. Computational Complexity

In this subsection, we investigate the computational costs of the off-line optimal and low-complexity sub-optimal policies. We used an Intel Core $i7-6700$, 2.6GHz CPU computer for performing the simulations. As it is proved in Section V, the computational complexity of off-line policies is a function of the number of users, events, and antennas. By setting $N_t = M$, in Fig. 7, we compare the average execution time of the proposed policies with the ZF technique through 100 trials versus number of events for different number of users. It is observed from Fig. 7 that implementing Algorithm 1 which is used to obtain the off-line optimal policies takes more time than Algorithm 3 which achieves the off-line low-complexity sub-optimal policies. The ZF precoding is faster than the proposed

This article has been accepted for publication in IEEE Transactions on Communications. This is the author's version which has not been fully edited and content may change prior to final publication. Citation information: DOI 10.1109/TCOMM.2022.3215997

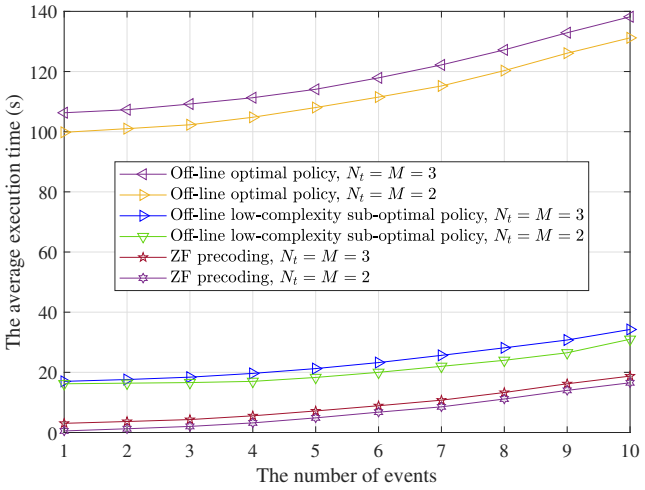

Fig. 7: A comparison among the proposed off-line optimal and low-complexity sub-optimal policies with the ZF precoding in terms of the average execution time over 100 trials.

policies because the beamforming vectors are predetermined, however, the performance of this approach highly depends on prior information regarding CSI. Indeed, when perfect CSI is not available, the potential ZF beamformers can no eliminate interference among the users, which makes the problem hard to solve. The performance obtained in terms of the throughput for the optimal and low-complexity sub-optimal solutions is comparable as shown in Figs. 2 and 6 and outperform the ZF technique. On the other hand, the complexity analysis in Table I and Fig. 7 demonstrate that the complexity of sub-optimal solution is less than the optimal ones up to 80 seconds. Indeed, there is a trade off between the complexity and accuracy of the optimal and sub-optimal policies. As we mentioned earlier, the solution of the optimal policy lies on the feasible set of the problem, however, the solution of the sub-optimal policy is a linear approximation of the optimal one which depends on ϵ_3 in Algorithm 3. Therefore, if the accuracy is highly important, the optimal policy can be exploited but with more complexity. For a better illustration, we do not plot the complexity of on-line policies because the complexity of the on-line policy is in the order of off-line policies by setting $i_0 = 1$ in ((19), the only difference is in number of events as we derived in Table I.

From the previous results, we can notice that the proposed policies can obtain better performance than the ZF precoding in terms of throughput for all the parameter settings. To provide a fair comparison, the execution time of the proposed policies is also compared with the ZF precoding. Note that the computational complexity of the proposed policies are functions of the number of users, antennas, and time slots. Therefore, changing these parameters can change the performance. However, since these parameters in many communication problems are fixed in practice and the main goal of this paper is to show the effects of energy balancing constraints on resource allocation policies, we fixed the number of users and antennas for all the simulations.

VII. Conclusion and Research Direction

In this paper, we study resource allocation policies in EH communication systems. We exploit the multi-antenna BS to take advantage of the channel diversity, however, this results in a non-convex optimization for the resource allocation because of the co-channel interference among users. To obtain the off-line optimal policy, we propose an iterative algorithm based on GLFP. We also present another iterative algorithm to achieve the off-line low-complexity sub-optimal policy. The on-line policies are studied, which only need the statistical CSI and EAI. The total computational complexity for the proposed approaches is derived. The simulation evaluations are provided to support our theoretic results.

Since the proposed policies solve non-convex resource allocation problems, we would like to suggest use our proposed techniques for more complicated non-convex problems such as EH dual-functional radar communication (DFRC) systems where a single platform accommodates both the radar and communication tasks simultaneously [28]. There is still lack of optimal and sub-optimal solutions for these access points because of non-convex constraints at both radar and communication sides.

Appendix A
Mathematical Preliminaries for GLFP

In this section, the necessary mathematical backgrounds for the GLFP technique [22] are provided in order to facilitate our algorithm's design for the optimal solution of problem (5).

Definition 1: For any two vectors, $\boldsymbol{y}, \boldsymbol{y}' \in \mathbb{R}^m$, we say $\boldsymbol{y}$ dominates $\boldsymbol{y}'$, if $\boldsymbol{y}' \leq \boldsymbol{y}$, i.e., $y'_i \leq y_i, \forall i \in \{1, \cdots, m\}$. For instance, in Fig. 8 (a), $\boldsymbol{z}_1$ dominates $\boldsymbol{z}_3$.

Definition 2: The hyper rectangle $[\boldsymbol{0}, \boldsymbol{z}] = \{\boldsymbol{x} | \boldsymbol{0} \leq \boldsymbol{x} \leq \boldsymbol{z}\}$ is called a box for given $\boldsymbol{z} \in \mathbb{R}^m_+$. Fig. 8 (a) shows three examples $\boldsymbol{z}_1$, $\boldsymbol{z}_2$, and $\boldsymbol{z}_3$ denoted by the black dashed lines.

Definition 3: For any set $\mathcal{T} \subset \mathbb{R}^m_+$, the union of the boxes constructed by $\mathcal{T}$, i.e., $[\boldsymbol{0}, \boldsymbol{z}]$ such that $\boldsymbol{z} \in \mathcal{T}$, is referred to a polyblock with the vertex set $\mathcal{T}$. For the example of Fig 8 (a) the vertex set of $\boldsymbol{z}_1$, $\boldsymbol{z}_2$ is denoted by the red dashed area.

Definition 4: A vertex $\boldsymbol{z} \in \mathcal{T}$ is called a proper vertex, if there exists no vertex in $\mathcal{T}$ dominates $\boldsymbol{z}$, i.e., for any $\boldsymbol{z}' \neq \boldsymbol{z} \in \mathcal{T}$, $\boldsymbol{z}' \geq \boldsymbol{z}$. In Fig. 8 (a), the vertex $\mathcal{T} = \{\boldsymbol{z}_1, \boldsymbol{z}_2\}$ is a proper vertex.

Definition 5: We call a set $\omega \subset \mathbb{R}^m$ normal, if for any $\boldsymbol{y} \in \omega$, the box $[\boldsymbol{0}, \boldsymbol{y}] \subset \omega$. In Fig. 8 (a), the black dashed area constructed by $\boldsymbol{z}_3$ is an example of a normal set. Note that the intersection of infinite normal sets is normal.

Fig. 8 (a) demonstrates an example of polyblock P constructed by the boxes $[\boldsymbol{0}, \boldsymbol{z}_1]$, $[\boldsymbol{0}, \boldsymbol{z}_2]$, and $[\boldsymbol{0}, \boldsymbol{z}_3]$. By using Definition 4, one can find that the vertex set of P is $\mathcal{T} = \{\boldsymbol{z}_1, \boldsymbol{z}_2\}$. The polyblock is a normal set because for any $\boldsymbol{z} \in P$, the box $[\boldsymbol{0}, \boldsymbol{z}] \in P$.

Definition 6: $\boldsymbol{y} \in \mathbb{R}^m_+$ that lies on the upper boundary set of the normal set $\omega \subset \mathbb{R}^m_+$, if $\alpha \boldsymbol{y} \in \omega, \forall \alpha < 1$ and $\alpha \boldsymbol{y} \notin \omega, \forall \alpha > 1$. The upper boundary set of ω is denoted by $\delta^+ \omega$. In Fig. 8 (a), the upper boundary of the normal set constructed by $\boldsymbol{z}_3$ is shown by black dashed line.

This article has been accepted for publication in IEEE Transactions on Communications. This is the author's version which has not been fully edited and content may change prior to final publication. Citation information: DOI 10.1109/TCOMM.2022.3215997

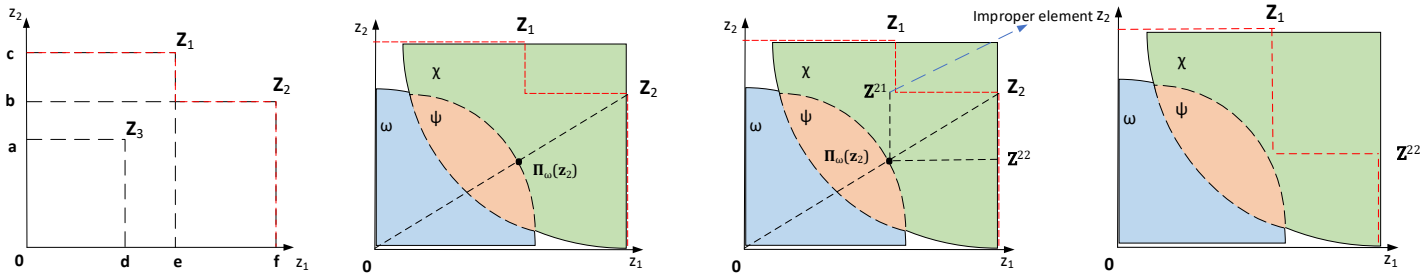

(a) (b) (c) (d)

Fig. 8: Fig. 8 (a) shows polyblock P constructed by the boxes $[\mathbf{0}, \boldsymbol{z}_1]$, $[\mathbf{0}, \boldsymbol{z}_2]$, and $[\mathbf{0}, \boldsymbol{z}_3]$ with the vertex set $\mathcal{T} = \{\boldsymbol{z}_1, \boldsymbol{z}_2\}$ in red dashed line. Figs. 8 (b, c, d) depict shrinking the ployblock over the set $\psi = \omega \cap \mathcal{X}$, where ω and $\mathcal{X}$ are normal and inverse normal sets, respectively.

Definition 7: For any normal set $\omega \subset \mathbb{R}^m_+$ and non-empty point $\boldsymbol{z} \in \mathbb{R}^m_+ \setminus \mathbf{0}$, the upper boundary of ω, i.e., $\delta^+\omega$, is met by a half-line from $\mathbf{0}$ to $\boldsymbol{z}$ at a unique point $\boldsymbol{\pi}^\omega(\boldsymbol{z})$, if $\boldsymbol{\pi}^\omega(\boldsymbol{z}) = \lambda \boldsymbol{z}, \quad \lambda = \sup\{\alpha \geq 0 |\ \alpha \boldsymbol{z} \in \omega\}$. Indeed, $\boldsymbol{\pi}^\omega(\boldsymbol{z})$ is the projection of $\boldsymbol{z}$ on the set ω. Note that $\boldsymbol{\pi}^\omega(\boldsymbol{z}) \geq \boldsymbol{z}$, i.e., $\lambda \geq 1$, if and only if $\boldsymbol{z} \in \omega$. In Fig. 8, $\Pi_\omega(\boldsymbol{z}_2)$ is the projection of $\boldsymbol{z}_2$ on $\boldsymbol{\omega}$.

For the remaining terms,

***Proposition** 1:* Consider $\Phi(\boldsymbol{z}) : \mathbb{R}^m_+ \to \mathbb{R}$ as an increasing function, the maximum of $\Phi(\boldsymbol{z})$ over the polyblock P with the vertex set $\mathcal{T}$ is achieved at one of the proper vertices of P. The maximum of $\Phi(\boldsymbol{z})$ over the normal set ω is obtained on the upper boundary set of ω.

Proof: Assuming that $\boldsymbol{z}^\star$ as the global maximum of $\Phi(\boldsymbol{z})$ over the polyblock P. If $\boldsymbol{z}^\star$ is not a proper vertex of P, there exists $\hat{\boldsymbol{z}}$ in $\mathcal{T}$ such that $\boldsymbol{z}^\star \leq \hat{\boldsymbol{z}}$, regarding the fact that $\Phi(\boldsymbol{z})$ is an increasing function, we have $\Phi(\boldsymbol{z}^\star) \leq \Phi(\hat{\boldsymbol{z}})$. Therefore, $\hat{\boldsymbol{z}}$ is a maximizer, which contradicts to $\boldsymbol{z}^\star$ as the global maximum of $\Phi(\boldsymbol{z})$. Similarly, if $\boldsymbol{z}^\star \in \omega$ is a maximizer of $\Phi(\boldsymbol{z})$ on ω, then $\boldsymbol{\pi}^\omega(\boldsymbol{z}^\star) \geq \boldsymbol{z}^\star$, consequently $\boldsymbol{z}^\star \in \delta^+\omega$. This concludes the proof.

***Proposition** 2:* Let us assume that ω as a normal closed set and $P \in \mathbb{R}^m_+$ a polyblock with the proper vertex set $\mathcal{T}$ contained ω. Suppose that $\hat{\boldsymbol{z}} \in \mathcal{T} \setminus \omega$, $\boldsymbol{\pi}^\omega(\hat{\boldsymbol{z}}) = \hat{\boldsymbol{y}}$, and $\mathcal{T}'$ a subset obtained from $\mathcal{T}$ such that $\mathcal{T}' \subset \{\boldsymbol{z} \in \mathcal{T} | \boldsymbol{z} \geq \hat{\boldsymbol{y}}\}$, let $\mathcal{T}^\star$ be a subset constructed from $\mathcal{T}$ by replacing $\boldsymbol{z} \in \mathcal{T}'$ with $\{\boldsymbol{z}^{1\star}, \cdots, \boldsymbol{z}^{m\star}\}$ such that $\boldsymbol{z}^{j\star} = \boldsymbol{z} - (z_j - \pi^\omega_j(\boldsymbol{z}))\boldsymbol{e}^j$, where $\boldsymbol{e}^j$ is j-th standard vector of $\mathbb{R}^m_+$ and $\pi^\omega_j(\boldsymbol{z})$ is the j-th element of $\boldsymbol{\pi}^\omega(\boldsymbol{z})$, then the polyblock $P^\star$ defined by the vertex set $\mathcal{T}^\star$ is smaller than $\mathcal{T}$ and still contains ω, i.e., $\omega \subset P^\star \subset P \setminus \{\hat{\boldsymbol{z}}\}$.

The proof of Proposition 2 is omitted because of space limitation, the details of the proof can be found in [22, Proposition 3]. Some of the elements in Proposition 2 might not be proper, however, they can be eliminated by the following technique. Consider the pair $(\boldsymbol{z}, \boldsymbol{z}^\star)$ such that $\boldsymbol{z} \in \mathcal{T}$ and $\boldsymbol{z}^\star \in \mathcal{T}^\star$. If $\boldsymbol{z}^\star \leq \boldsymbol{z}$, then remove $\boldsymbol{z}^\star$. We show this procedure in Figs. 8 (b, c, d).

Definition 8: A set $\mathcal{X}$ is called reverse normal set if $\boldsymbol{y}' \geq \boldsymbol{y}$ for $\boldsymbol{y} \in \mathcal{X}$ implies $\boldsymbol{y}' \in \mathcal{X}$. For example, in Fig. 8, the green area is a inverse normal set.

***Proposition** 3:* Let us consider $\Phi(\boldsymbol{z}) : \mathbb{R}^m_+ \to \mathbb{R}$ as an increasing function, the maximum $\Phi(\boldsymbol{z})$ over $\psi = \omega \cap \mathcal{X}$, where ω and $\mathcal{X}$ are normal and inverse normal closed sets, respectively, if it exists, is obtained at $\delta^+\psi$.

Proof: If $\psi \neq \emptyset$, because interior points of the set ω is not empty, then we have $\psi \setminus \{\mathbf{0}\} \neq \emptyset$. Since $\Phi(\boldsymbol{z})$ is an increasing function, if there exists a maximizer $\boldsymbol{z}^\star$ for $\Phi(\boldsymbol{z})$ over ψ, it should not be equal to zero, i.e, $\boldsymbol{z}^\star \neq 0$. By using Definition 7, it is known that $\delta^+\omega$ is met at the half-line from $\mathbf{0}$ through $\boldsymbol{z}$, let us consider $\boldsymbol{y} = \boldsymbol{\pi}^\omega(\boldsymbol{z})$. Based on $\boldsymbol{z} \in \omega$, we have $\boldsymbol{z} \leq \boldsymbol{y}$, thus $\boldsymbol{y} \in \mathcal{X}$ as $\boldsymbol{z} \in \mathcal{X}$. This implies that $\boldsymbol{y} \in \delta^+\psi$. Moreover, $\Phi(\boldsymbol{z})$ is an increasing function, thus, $\Phi(\boldsymbol{y}) \geq \Phi(\boldsymbol{z})$ because of $\boldsymbol{y} \geq \boldsymbol{z}$. This concludes that $\boldsymbol{y}$ is a maximizer of $\Phi(\boldsymbol{z})$ over the set ψ.

Appendix B
Proof of Theorem 1

A sequence $\{\boldsymbol{z}_j\}$, $\forall j = \{1, 2 \cdots\}$ is generated by Algorithm 1 where each element can be obtained by the optimization problem in seven line of Algorithm 1. One can always find a sub-sequence $\{\boldsymbol{z}_{t_n}\}$ such that $\boldsymbol{z}_{t_1} = \boldsymbol{z}_1 - (z_{1i_0} - \pi^\omega_{i_0}(\boldsymbol{z}_1))\boldsymbol{e}^{i_0}$, $\boldsymbol{z}_{t_{n+1}} = \boldsymbol{z}_{t_n} - (z_{t_n i_n} - \pi^\omega_{i_n}(\boldsymbol{z}_{t_n}))\boldsymbol{e}^{i_n}$, where $1 < t_1 < t_2 < \cdots < t_n < \cdots$ and $z_{t_n i_n}$ denotes the i_n-th element of $\boldsymbol{z}_n$. Note that $\boldsymbol{z}_{t_n+1}$ differs from $\boldsymbol{z}_{t_n}$ only in the index i_n. A series of projections of $\boldsymbol{z}_1$ is used to obtain the sequence $\{\boldsymbol{z}_{t_n}\}$ which might not be adjacent as projections of other vertices also occur. Regarding the fact that $\boldsymbol{\pi}^\omega(\boldsymbol{z}_{t_n}) \leq \boldsymbol{z}_{t_n}$, one can show that $\boldsymbol{z}_1 \geq \boldsymbol{z}_{t_1} \geq \cdots \geq \boldsymbol{z}_{t_n} \geq \cdots \geq 2^{\bar{R}^{\mathrm{q}}}$. Therefore, $\lim_{n\to\infty} \|\boldsymbol{z}_{t_{n+1}} - \boldsymbol{z}_{t_n}\|_2 = 0$. It is known from above that $\boldsymbol{z}_{t_{n+1}}$ and $\boldsymbol{z}_t$ differ only at i_n-th element, thus, we have $\|\boldsymbol{z}_{t_{n+1}} - \boldsymbol{z}_{t_n}\|_2 = \boldsymbol{z}_{t_{n+1} i_n} - \boldsymbol{z}_{t_n i_n} = \boldsymbol{z}_{t_{n+1} i_n} - \pi^\omega_{i_n}(\boldsymbol{z}^t) \to 0$, for $n \to \infty$. On the other hand, we have $\boldsymbol{\pi}^\omega(\boldsymbol{z}_{t_n}) = \lambda^{t_n} \boldsymbol{z}_{t_n}$, thus, $\lim_{n\to\infty} \lambda^{t_n} \to 1$, leading to $\lim_{n\to\infty} \boldsymbol{z}_{t_n} \to \boldsymbol{\pi}^\omega(\boldsymbol{z}_{t_n})$, where implies that the sub-sequence $\{\boldsymbol{z}_{t_n}\}$ converges to the upper boundary of the set ψ. Thus, it is a maximizer and the global optimal solution of problem P_1. The convergence of the sub-sequence of $\{\boldsymbol{z}_{t_n}\}$ concludes the convergence of Algorithm 1 to the optimal solution because Algorithm 1 is stopped when the optimal solution of problem P_1 is obtained.

APPENDIX C
PROOF OF THEOREM 2

Let us denote t_3 and $O(\boldsymbol{p}^{t_3})$ as the iteration step and objective value of problem (12) at the t_3-th iteration, respectively. Problem (12) is optimally solved in the third step of each iteration, thus, we have $O(\boldsymbol{p}^{t_3}) \leq O(\boldsymbol{p}^{t_3+1})$, where shows that the objective value of problem (12) is non-decreasing and upper bounded by a finite value. Consequently, Algorithm 3 is convergent. Numerical evaluations in Section VI also reveal that proposed Algorithm 3 converges quickly.

ACKNOWLEDGMENT

This project has received funding from the European Union's Horizon 2020 research and innovation program under the Marie Skłodowska-Curie grant agreement No 812991.

REFERENCES

[1] J. Ma, S. Zhang, H. Li, F. Gao, and S. Jin, "Sparse bayesian learning for the time-varying massive mimo channels: Acquisition and tracking," *IEEE Transactions on Communications*, vol. 67, no. 3, pp. 1925–1938, 2018.

[2] A. F. Molisch and M. Z. Win, "Mimo systems with antenna selection," *IEEE microwave magazine*, vol. 5, no. 1, pp. 46–56, 2004.

[3] E. Vlachos and J. Thompson, "Energy-efficiency maximization of hybrid massive mimo precoding with random-resolution dacs via rf selection," *IEEE Transactions on Wireless Communications*, vol. 20, no. 2, pp. 1093–1104, 2020.

[4] A. Li, C. Masouros, F. Liu, and A. L. Swindlehurst, "Massive mimo 1-bit dac transmission: A low-complexity symbol scaling approach," *IEEE Transactions on Wireless Communications*, vol. 17, no. 11, pp. 7559–7575, 2018.

[5] O. Mehanna, N. D. Sidiropoulos, and G. B. Giannakis, "Joint multicast beamforming and antenna selection," *IEEE Transactions on Signal Processing*, vol. 61, no. 10, pp. 2660–2674, 2013.

[6] J. Yang and S. Ulukus, "Optimal packet scheduling in a multiple access channel with energy harvesting transmitters," *Journal of Communications and Networks*, vol. 14, no. 2, pp. 140–150, 2012.

[7] A. A. Nasir, X. Zhou, S. Durrani, and R. A. Kennedy, "Relaying protocols for wireless energy harvesting and information processing," *IEEE Transactions on Wireless Communications*, vol. 12, no. 7, pp. 3622–3636, 2013.

[8] J. Yang, O. Ozel, and S. Ulukus, "Broadcasting with an energy harvesting rechargeable transmitter," *IEEE Transactions on Wireless Communications*, vol. 11, no. 2, pp. 571–583, 2011.

[9] J. Yang and S. Ulukus, "Optimal packet scheduling in an energy harvesting communication system," *IEEE Transactions on Communications*, vol. 60, no. 1, pp. 220–230, 2011.

[10] K. Tutuncuoglu and A. Yener, "Optimum transmission policies for battery limited energy harvesting nodes," *IEEE Transactions on Wireless Communications*, vol. 11, no. 3, pp. 1180–1189, 2012.

[11] B. Devillers and D. Gündüz, "A general framework for the optimization of energy harvesting communication systems with battery imperfections," *Journal of Communications and Networks*, vol. 14, no. 2, pp. 130–139, 2012.

[12] O. Ozel, K. Tutuncuoglu, J. Yang, S. Ulukus, and A. Yener, "Transmission with energy harvesting nodes in fading wireless channels: Optimal policies," *IEEE Journal on Selected Areas in Communications*, vol. 29, no. 8, pp. 1732–1743, 2011.

[13] O. Orhan, D. Gündüz, and E. Erkip, "Energy harvesting broadband communication systems with processing energy cost," *IEEE Transactions on Wireless Communications*, vol. 13, no. 11, pp. 6095–6107, 2014.

[14] D. W. K. Ng, E. S. Lo, and R. Schober, "Energy-efficient resource allocation in ofdma systems with hybrid energy harvesting base station," *IEEE Transactions on Wireless Communications*, vol. 12, no. 7, pp. 3412–3427, 2013.

[15] Z. Zhou, H. Yu, S. Mumtaz, S. Al-Rubaye, A. Tsourdos, and R. Q. Hu, "Power control optimization for large-scale multi-antenna systems," *IEEE Transactions on Wireless Communications*, vol. 19, no. 11, pp. 7339–7352, 2020.

[16] C. Park and P. H. Chou, "Ambimax: Autonomous energy harvesting platform for multi-supply wireless sensor nodes," in *2006 3rd annual IEEE communications society on sensor and ad hoc communications and networks*, vol. 1, pp. 168–177, IEEE, 2006.

[17] P. Blasco, D. Gunduz, and M. Dohler, "A learning theoretic approach to energy harvesting communication system optimization," *IEEE Transactions on Wireless Communications*, vol. 12, no. 4, pp. 1872–1882, 2013.

[18] J. Huang, B. Yu, C.-c. Xing, T. Cerny, and Z. Ning, "Online energy scheduling policies in energy harvesting enabled d2d communications," *IEEE Transactions on Industrial Informatics*, 2020.

[19] S. Boyd and L. Vandenberghe, *Convex optimization*. Cambridge university press, 2004.

[20] I. Rubin, "Message delays in fdma and tdma communication channels," *IEEE Transactions on Communications*, vol. 27, no. 5, pp. 769–777, 1979.

[21] J. Ma, S. Zhang, H. Li, N. Zhao, and V. C. Leung, "Interference-alignment and soft-space-reuse based cooperative transmission for multi-cell massive mimo networks," *IEEE Transactions on Wireless Communications*, vol. 17, no. 3, pp. 1907–1922, 2018.

[22] N. T. H. Phuong and H. Tuy, "A unified monotonic approach to generalized linear fractional programming," *Journal of Global Optimization*, vol. 26, no. 3, pp. 229–259, 2003.

[23] Y. Chen, W. Feng, R. Shi, and N. Ge, "Pilot-based channel estimation for af relaying using energy harvesting," *IEEE Transactions on Vehicular Technology*, vol. 66, no. 8, pp. 6877–6886, 2017.

[24] I. Valiulahi, M. Javidsharifi, M. Virgili, and C. Masouros, "D3. 1–energy models and optimisation framework: Phase 1."

[25] M. Grant, S. Boyd, and Y. Ye, "cvx users' guide," *online: http://www. stanford. edu/˜ boyd/software. html*, 2009.

[26] S. Schaible, "Fractional programming," in *Handbook of global optimization*, pp. 495–608, Springer, 1995.

[27] E. Karipidis, N. D. Sidiropoulos, and Z.-Q. Luo, "Quality of service and max-min fair transmit beamforming to multiple cochannel multicast groups," *IEEE Transactions on Signal Processing*, vol. 56, no. 3, pp. 1268–1279, 2008.

[28] I. Valiulahi, C. Masouros, A. Salem, and F. Liu, "Antenna selection for energy-efficient dual-functional radar-communication systems," *IEEE Wireless Communications Letters*, 2022.